Journal of Interfaces, Thin films, and Low dimensional systems 7 (1) Summer and Autumn (2023) 721-729

Fractal analysis of GISS Earth's surface temperature data

Scientific research paper

M. Lak[1], S. Hosseinabadi[2*], A. A. Masoudi[1*]

[1]*Department of Condensed Matter Physics, Faculty of Physics, Alzahra University, Tehran, Iram*

[2]*Department of Physics, East Tehran Branch, Islamic Azad University, Tehran, Iran*

ARTICLE INFO

Article history:
Received 30 January 2024
Revised 5 March 2024
Accepted 9 March 2024
Available online 18 March 2024

Keywords
Multifractal detrended fluctuation analysis
Long term correlation
GISTEMP

ABSTRACT

Rising temperature plays a significant role in global warming and has consequences on human health conditions, ecosystems, energy etc. Hence, studying and monitoring its states will help scientists seek solutions to prevent its harmful effects. In this study, we investigated the Earth's surface temperature anomaly fluctuations by fractal analysis. We gathered the temperature anomaly dataset including land and sea surface temperatures. The maximum, minimum, and average temperatures of each year were investigated. Furthermore, we used multifractal detrended fluctuation analysis (MF-DFA) to figure out whether these fluctuations appear randomly or follow a rule. By removing the trend and applying the MFDFA on data, the Hurst exponent obtained as $H = 0.83 \pm 0.02$, which means a positive long-term correlation exists among data that causes the increasing trend. Besides, the scalability exponent, $\tau(q)$, and the singularity spectrum, $f(\alpha)$, were plotted, and both of them approved the multifractality for the temperature dataset. To discover what is the cause of multifractality, the main, shuffling, and surrogating data were evaluated. The results depicted both the long correlation for small and large fluctuations and the distribution deviation from Gaussian distribution have effects on the multifractal behavior of the data, but according to the graph, the long correlation is more effective.

1 Introduction

One of the most prominent criteria for agriculture, environment, and meteorology is the temperature of the Earth [1, 2], which is also the most significant component of global warming [3]. When the Sun's rays reach the Earth's surface, a few percent of it reflects, and the remaining percent is absorbed by molecules of oceans and air, which helps Earth to get warmer and be a comfortable place for living [3]. Over the past 100 years, the Earth has become abnormally warmer by about 0.6 degrees Celsius [4] which is the reason for severe drought, famine, flood. This will predict global warming in ~ 2100 which may cause more natural disasters, severe droughts, scorching heat, and terrible storms [4].

According to the news, more countries are worried about climate change and global warming because this case affects life on land and sea. So it is noteworthy that the importance of climate change and research on this issue leads to understanding and predicting the future weather while being aware of how badly natural disasters will occur and how to reduce their impacts. Scientists use data from plants, glaciers, and other samples to determine the reasons for these phenomena, and their researches confirm that human activities have

*Corresponding author.
Email address: Sakineh.Hosseinabadi@iau.ac.ir, Masoudi@alzahra.ac.ir
DOI: 10.22051/jitl.2024.46341.1106

a significant impact [5]. During the COVID-19 lockdown, climate change seemed to heal due to the less demand for conventional energy sources [6], which can be a clue to use more renewable energy. Earth's surface temperature is obtained by combining land surface temperature and ocean surface temperature. Satellite observational results may also include.

In this paper, we investigate the dataset collected by NASA's Goddard Institute for Space Studies[1] (GISTEMP), which is available at [7]. Other organizations also collect temperature datasets, but the GISS has more comprehensive coverage than the others (the cover of the GISS is 99 percent) [8, 9]. It is noticeable that none of these organizations measure the absolute temperature but measure the temperature anomaly. The temperature anomaly is considered as follows: whenever in a climatic period, for example, in 30 years, the statistical temperatures do not differ significantly and present stable behavior, this period considers the climatic norm. When the temperature values deviate from this norm, they are considered an anomaly. The measuring temperature during 1951-1980 is the climatic norm period [8]. The reason for using temperature anomalies is that the actual temperature measurements are often difficult to collect, many areas in the world have a small number of recording stations, and temperature inevitably estimates in larger zones, which reduces the accuracy of the measurement. The usage of anomaly temperature provides a more accurate description in a larger zone than the actual temperature [9].

Several statistical examinations have been implemented on GISTEMP data to find the effects of rising temperatures. For instance, on underlying tectonic movements through earthquakes, which revealed there is a bidirectional causality between them [10] or discovering a cross-correlation between surface temperature and solar activity which deducted how many years solar activity influences surface temperature [11]. Moreover, numerous statistical modelings have been performed, like auto-regression [12], Bayesian [13], and Sliced Functional Time Series [14] models on the GISTEMP data to find the best fitting models and capture the behavior of time series. Generally, analyzing the specific region's temperature of the world [15, 16, 17] or the global temperature [18, 19] deducted two same results. The first is that the temperature dataset is non-stationary, and the second is a positive long-term correlation between data. By just plotting the data based on time Fig. 1a, it is observed that the temperature rises considerably, which by previous explorations, we know has some form of devastating consequences such as the melting of glaciers and rising sea levels, the scarcity of healthy water and food, the extinction of animal species, and many others [2].

Many natural processes surrounding us are not defined as simple as linear equations. They are classified as complex systems because understanding their behavior is complicated. The approach to studying them is based on nonlinear equations. One of these processes is the time series, in which the variables change through the time scale. Due to the variation of Earth's surface temperature anomaly values during the time, they are as the time series classification. Fractal analysis is a beneficial tool to investigate time series fluctuations [20]. Fractals were first introduced in the late 1960s by B. B. Mandelbrot and used for objects with complex geometry when no proper dimensions were found [21].

Fractal analysis helps us understand important scientific concepts such as the growth of bacteria, patterns of snowflakes, brain waves, et Cetra, and investigate their causes of behaviors [22]. Here we use the multi-fractal detrended fluctuation analysis (MF-DFA) because it is an almost complete method for investigating single-fractal or multi-fractal behaviors, the cause of the behaviors, and the type of the dataset correlation [22].

2 Methodology

Fractal geometry consists of algorithms that are converted into regular shapes, structures, and images by computers. The foundation of fractal geometry depends on the assumption that natural figures are identical and created from the lawful repetition of an initial block [23]. The random processes in nature generate self-similar or self-affine fractals in which any irregularity results in multi-affinity. Time series of fluctuating values of a stock price, atmospheric pressure and

[1] GISS

temperature, relative humidity, and hemodynamics are some examples [22, 23].

2.1 Multi-fractal detrended fluctuation analysis

The detrended fluctuation analysis of multi-fractal was obtained in five steps.

Step 1: we need to have a series of data (here is the Earth's surface anomaly temperature), in which the values vary through the time $T(i)$, in the length of N (i counts the number of the months) and its profile was calculated as follows [23, 24]:

$$Y(j) = \sum_{i=1}^{j}[T(i) - \langle T\rangle] = \sum_{i=1}^{j}\tilde{T}_i, j = 0,1,2,\dots,N. \quad (1)$$

Step 2: Divide the profile length $Y(i)$ into $N_s = int\left(\frac{N}{s}\right)$ non-overlapping segments of the same range as s. Since the length of the series is not a multiple of the considered time scales s, the same method is repeated from the end of the series, which means the number of the segment is $2N_s$ [24].

Step 3: Using the least-squares fit on the data profile to compute a local trend for each $2N_s$ segment. Then, calculate the variance for each segment by Eq. (2) and Eq. (3) [24];

$$F^2(s,\nu) = \frac{1}{s}\sum_{i=1}^{s}\{Y[(\nu-1)s+i] - y_\nu(i)\}^2, \nu = 1,\dots,N_s, \quad (2)$$

$$F^2(s,\nu) = \frac{1}{s}\sum_{i=1}^{s}\{Y[N-(\nu-N_s)s+i] - y_\nu(i)\}^2, \nu = N_s+1,\dots,2N_s. \quad (3)$$

Linear, quadratic, cubic, and higher order polynomials can be utilized in the fitting method, which the corresponding methods are thus called MFDFA1, MFDFA2, MFDFAm (m is the mth order of the trends of the profile and is equivalent to the $(m-1)$th order of the main data) and must be eliminated. Thus, a comparison of the results for different orders of DFA allows us to estimate the type of the polynomial trend in the time series [24, 25, 26].

Step 4: Average throughout the segments to get the qth order of the fluctuations function:

$$F_q(s) = \left\{\frac{1}{2N_s}\sum_{\nu=1}^{2N_s}[F^2_{DFAm}(\nu,s)]^{\frac{q}{2}}\right\}^{\frac{1}{q}}. \quad (4)$$

The DFA method is retrieved for $q = 2$. $F_q(s)$ depends on a timescale (s) for different values of q. Thereupon, steps 2, 3, and 4 must be repeated for some different s to observe that by increasing s the values of $F_q(s)$ also increase. Additionally, $F_q(s)$ relies on the m-order of DFA. Hence, $F_q(s)$ is only defined for $s \geq m+2$ [24,26].

Step 5: Determine the scaling behavior of the fluctuation function by analyzing the log-log plot of $F_q(s)$ vs s for different values of q. If the time series $T(i)$ are long-term power-law correlated, $F_q(s)$ increases as a power-law for each value of s [24]:

$$F_q(s) \sim s^{h(q)}. \quad (1)$$

The value of $h(q)$ for when $q \to 0$ can not be determined directly using the average method in Eq. (4) because of the diverging exponent. Instead, a logarithmic averaging procedure has to be employed;

$$F_0(s) = exp\frac{1}{4N_s}\sum_{\nu=1}^{2N_s} ln[F^2(\nu,s)] \sim s^{h(0)}. \quad (6)$$

For large scales $s > \frac{N}{4}$, $F_q(s)$ becomes unreliable because the number of segments N_s in step 4 becomes very small. Thus, scales $s > \frac{N}{4}$ should be excluded from the fitting procedure determining $h(q)$. $h(q)$ is the generalized Hurst exponent, which for monofractal time series is independent of q, whereas, for multifractal time series, $h(q)$ varies with q. For $q = 2$, the generalized Hurst exponent is exactly equal to the Hurst exponent that provides information about the average fluctuation of the series [25, 26]. For the monofractal series, the $H = h(q=2)$, and for the multifractal series, the Hurst exponent obtains $H = h(q=2) - 1$ [24, 26]. Depending on $h(q=2)$, the series categorized into; (i) $0 < h(q=2) < 0.5$ which is for an anti-persistent long-range correlated (negative long-term memory), (ii)

$h(q=2)=0.5$ is for uncorrelated distribution, and (iii) $0.5<h(q=2)<1$ is for a persistent long-range correlated (positive long term memory) [24]. For $q>0$, the $h(q)$ describes the scaling behavior of the segments with large fluctuations. In contrast, for $q<0$, the $h(q)$ describes the scaling behavior of the segments with small fluctuations [24].

The classical multifractal scaling exponent $\tau(q)$ (it is also known as Renyi scaling exponent) is defined by the standard partition function-based formalism, which is related to the generalized Hurst exponent as [26];

$$h(q)=\frac{1+\tau(q)}{q}, \quad (7)$$

When $\tau(q)$ depends linearly on q it demonstrates the mono-fractality, otherwise, it is multifractality [24].

Singularity spectra $f(\alpha)$ is another way to characterize the multifractality of the series and is related to $\tau(q)$ with the Legendre transform [24, 26]. α is Holder exponent, that displays the singularity strength, and is obtained by using Eq. (7) [24];

$$\tau(q)=qh(q)-1, \quad (2)$$

$$f(\alpha)=q\alpha-\tau(q), \quad (3)$$

$$f(\alpha)=q[\alpha-h(q)]+1, \quad (4)$$

and

$$\alpha=h(q)+qh'(q). \quad (5)$$

If the α results in a single value, it denotes monofractal behavior, and if it results in different values (which leads to a spectrum) for different parts of a structure it denotes multifractality [26]. The range of the Holder exponent is calculated in the following ways;

$$\alpha_{min}=\lim_{q\to-\infty}\left(\frac{\partial\tau(q)}{\partial q}\right), \quad (12)$$

$$\alpha_{min}=\lim_{q\to-\infty}\left(\frac{\partial\tau(q)}{\partial q}\right). \quad (13)$$

3 Results and discussion

At first, we examined the data to observe its initial conditions, so we plotted the Earth's surface average temperature anomaly data vs the monthly time scale, which was collected from January 1880 to December 2023. Figure 1a shows a considerably increasing trend in recent decades.

We also calculated the annual maximum and minimum temperature, the average temperature, and the difference between the maximum and minimum. As shown in Fig. 2, the red line is the minimum temperature of the years, and the green line is the maximum. The blue line is the average temperature during the years, which as we can see, is not the same value for all the timescales and it means our data are non-stationary. The black line is the subtraction of the maximum and minimum temperatures. The black line shows no consistent upward or downward trend over the entire period, just a variation around the mean value.

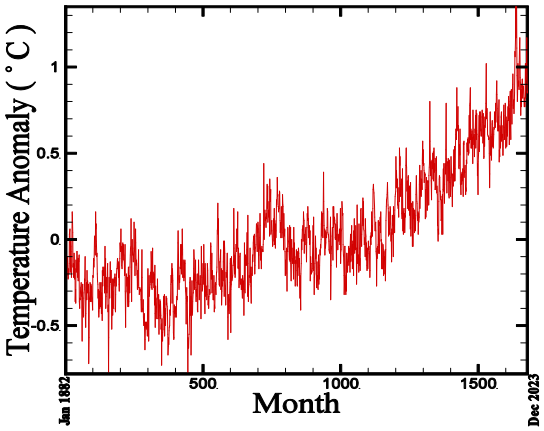

(a)

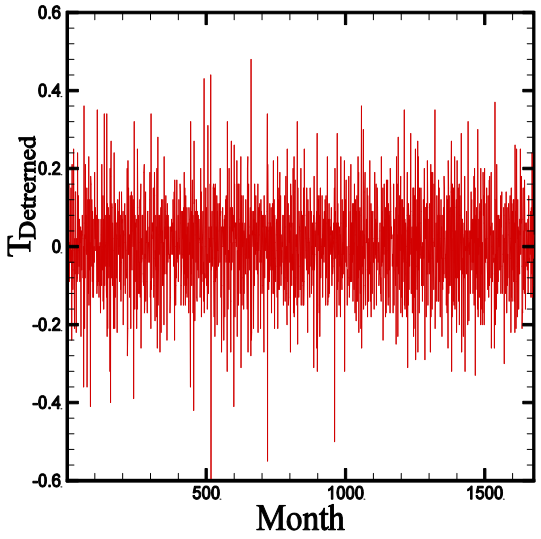

(b)

Figure 1. (a) The GISS Earth temperature anomalies data averaged in months from January 1880 to December 2023. (b) For differentiated data as $T_{Detrended} = T_i - T_{i-1}$.

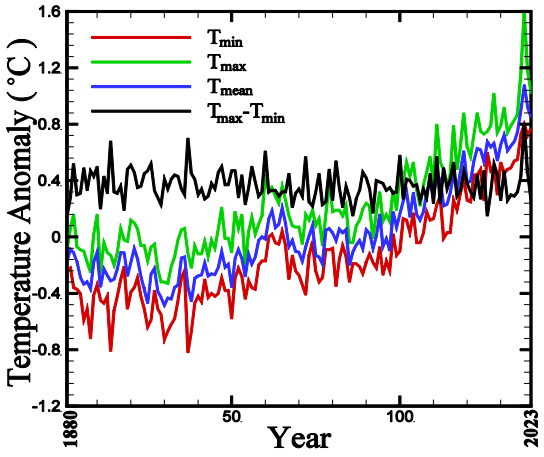

Figure 2. The trend of the annual minimum and maximum temperature.

What we looked for was the information that the temperature fluctuation shows. In this order, the uprising trend of the data should be eliminated to probe the fluctuations. To make the data stationary, the values of the trend function in each interval time were calculated and the values of time series data were subtracted from the corresponding data in the trend line equation. This difference is considered a new value for the time series. With this method, the average data and their variance are fixed and the trend of the data is also removed, Fig. 1b.

3.1 Fractal behavior

As mentioned in section 2, we had to do 5 steps on the detrended data to plot the log-log of the fluctuation function vs the scale s for different orders of q, which is shown in Fig. 3. There are no crossover timescales on the graph, which means the data are stationary and there is no competition between the noise and trend [24, 25, 26]. As it is mentioned in the essay, the increased linear trend was removed, but it is not recognizable whether there are any trends in the data. Plotting the fluctuation function and observing no crossover would assure us that there is no trend in the data and the data is now stationary. If there were crossovers that caused changes in the fluctuation function's behavior, then there was a sinusoidal trend in the data and there must be methods to cancel this trend [References 24, 25, and 26]. For each q a line could be fitted easily and the slopes are different with respect to q, which means multifractal behavior in the data. According to Section 2.1 The slope of the fitted line for $q = 2$ in Fig. 3 depicts the Hurst exponent [25, 26].

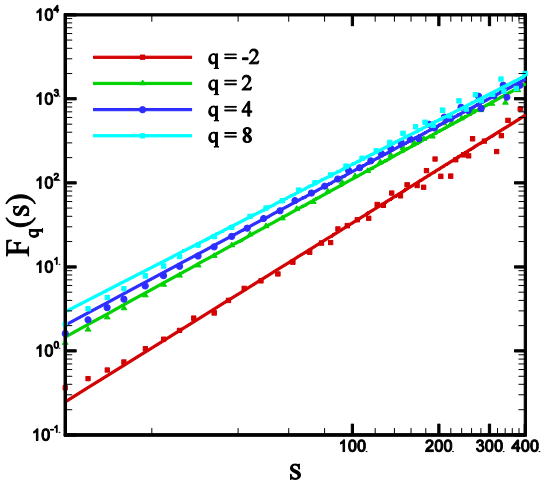

Figure 3. Logarithmic diagram of the fluctuation $F_q(s)$ with respect to s for different values of q moments.

The generalized Hurst exponent, $h(q)$, was calculated (according to Eq. 4), and its graph is plotted in Fig. 4. According to section 2.1. and the fact that the process under examinations is non-stationary, the Hurst exponent is as follows

$$H = h(q) - 1 = 0.83 \pm 0.02. \quad (14)$$

As the description of Hurst exponent in section 2, the Earth's surface temperature has a positive long-term correlation. A long-term correlation means two variables move in tandem in the same direction. When one variable tends to increase as the other variable increases or one variable tends to decrease while the other decreases. Meanwhile, as time passes, the temperatures tend to increase, which means today's temperature has a definite effect on future temperatures. As we know, $q < 0$ indicates small fluctuations, and $q > 0$ demonstrates large fluctuations [24, 26]. As it is apparent in Fig. 4, while the values of q increase, the $h(q)$ decreases. It means that there is a strong dependency (an inverse relation) among $h(q)$ and q for monthly, minimum, and maximum annual temperatures, it could be estimated by the multi-fractal behavior [24, 25, 26].

It is noticeable that as the main fractal pattern admits, the behavior of the generalized Hurst's exponent is independent of q for any monofractal process. This is because of the identical behavior of variances $F^2_{DFAm}(v, s)$ for all the segments.

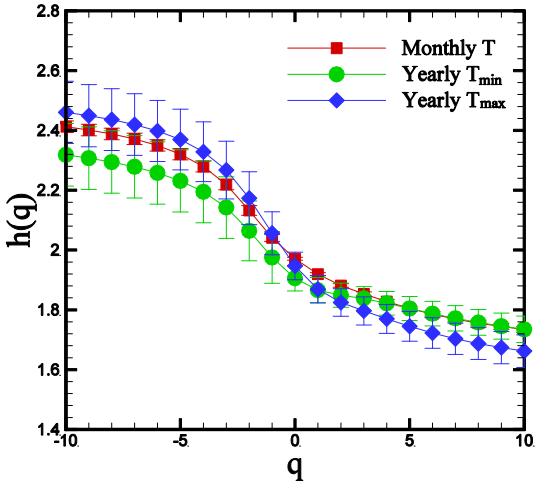

Figure 4. Generalized Hurst exponent diagram for monthly data and annual maximum and minimum data

To genuinely test the multi-fractal behavior, we also examined the scalability exponent and singularity spectrum (Holder spectrum). The generalized Hurst exponent, introduced by the MF-DFA method, is related to the multi-fractal scalability exponent as Eq. (8)[24].

In Fig. 5 (plotted for monthly, minimum, and maximum annual), the graph has a different slope for positive and negative q, which indicates that the temperature data pursues the multi-fractal behavior. Moreover, the singularity spectra figure for monthly, minimum, and maximum annual was plotted. In Fig. 6, the singularity spectrum has a wider length for maximum annual temperature than monthly and minimum annual temperature, which displays that the multi-affinity strength is greater for yearly max temperature time series [24, 26].

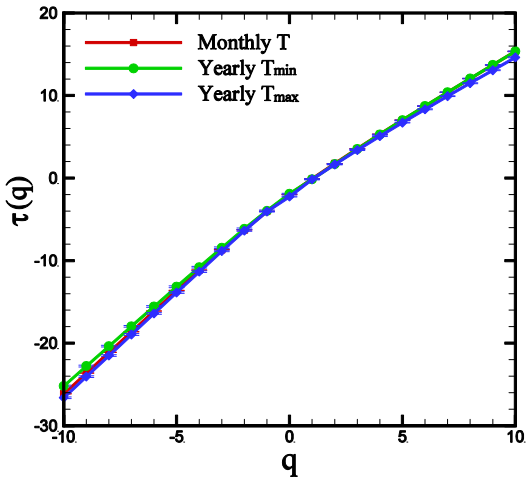

Figure 5. Multi-fractal scalability exponent diagram for the main data and annual maximum and minimum data.

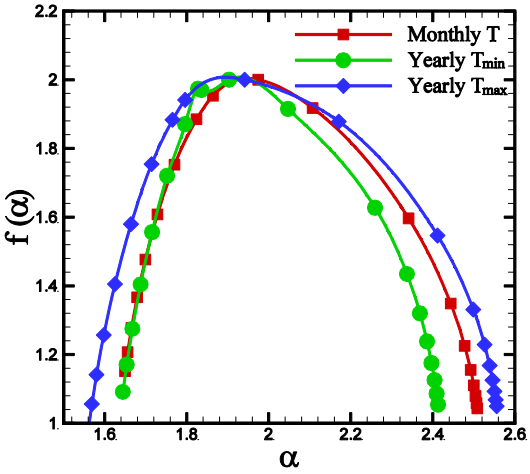

Figure 6. The singularity spectrum of monthly average temperature data, annual maximum average temperature, and annual minimum average temperature.

3.2 The origin of multi-fractal behavior

Due to the strong dependence of the generalized Hurst exponent on q, the difference in the slope of the $\tau(q)$ versus q, and the spectrum of the $f(\alpha)$ versus α (not a single value), it is deduced that the temperature data has a multifractal behavior. Then, the cause of multifractality had to be recognized. There are two types of multifractality in time series, which both require a multitude of scaling exponents for small and large fluctuations, one can be due to a broad probability density function of the data, and the other can be due to different long-correlations for all the range of fluctuations [24].

To find the origin of different long-correlations for small and large fluctuations, the shuffled data is utilized. If the shuffled data makes the multifractality disappear, the generalized Hurst exponent becomes independent of q. Shuffling data does not change the distribution function of the data, but by putting values in random orders their correlations change [23, 24]. The other reason for the multifractality is when the probability density distribution function (PDF) deviates from the Gaussian function. In this case, the data had to be surrogated, which makes the distribution function of the Earth's surface anomaly temperature data converted to Gaussian, the multifractal behavior disappeared, and the generalized Hurst exponent does not rely on q. The correlation does not change, but the distribution function changed to the Gaussian distribution [23, 24]. In this case, some steps have to be taken [24, 26]:

I: Transfer the data by Fourier transforming to Fourier space:

$$T(\nu) = F\{T(t)\} = \sum_{n=0}^{N-1} T(t_n) e^{2\pi i \nu t_n}. \qquad (15)$$

II: Multiply the coefficients of this transform by $e^{i\phi(\nu)}$ ($\phi(\nu)$ with a uniform distribution in the range $[0.\ 2\pi]$).

$$\tilde{T}(\nu) = T(\nu) e^{i\Phi(\nu)}. \qquad (16)$$

III: Gaussian data will be obtained by inverse Fourier transform:

$$\tilde{T}(t_n) = F^{-1}\{\tilde{T}(\nu)\}. \qquad (17)$$

The range of the surrogate data is the same as the original data.

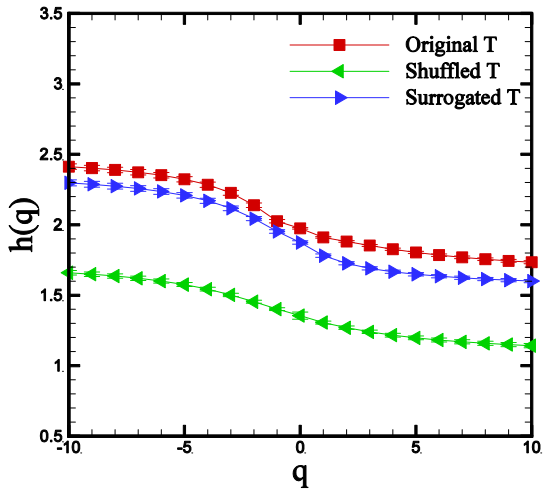

Figure 7. Generalized Hurst exponent diagram for the original data, surrogated data, and shuffled data.

Using the two mentioned methods, we investigate which one is the cause of the multi-fractal behavior. Either of these methods exhibits the generalized Hurst exponent becoming independent of q as the reason for fractality. If both cause the multi-fractal behavior, then the generalized Hurst exponent for both shuffled and surrogated data depends on q weaker than the original series [24]. Figure 7 shows the generalized Hurst exponent versus q values for the main, shuffled, and surrogated series. As it is apparent, for all three datasets, the generalized Hurst exponent depends on q, which means both the long correlation between the data and the deviation of the probability density distribution function are the reasons for the multi-fractal behavior in the investigated Earth's surface temperature time series, but the long-correlation has more effect on multifractality because its line is closer to the original data line.

4 Conclusions

In this study, we investigated the collected monthly average Earth's surface temperature anomaly dataset, which includes land surface and sea surface temperatures from NASA GISS. In a comparison of the variety of dataset collections, we selected GISTEMP because it has more complete coverage than others. To survey how the data fluctuate throughout time and what information the data possesses, we used the multifractal analysis because it is a convenient method for nonstationary time series. The results demonstrated that the data had an increasing trend which means the Earth's temperature is rising. To investigate the fractal behavior of the data, we removed the uprising trend of the data, where a power law behavior indicating the fractal feature was observed in the fluctuation function of the temperature set. The value of Hurst exponent was calculated as $H = 0.83 \pm 0.02$ which means the fluctuations are not random and a positive correlation exists among them where this correlation can increase the future temperature. Besides, more calculations exhibited multifractal feature in the temperature dataset, which indicated that the correlations are not the same in the small and large scales and the strength of multi-affinity was determined.

To find what causes the multi-affinity in Earth's surface temperature time series, two methods were tested, the first was to make the correlation of the data go away by shuffling data, and the second was to transform the distribution function of the data to the Gaussian function by surrogating data, and finally plot the generalized Hurst exponent for both of them and compare them with the generalized Hurst exponent for original data. In conclusion, both approaches show multi-affinity which indicate that both different correlations and distribution function deviation from the Gaussian one are the source of multi-affinity feature in the GISS temperature data-sets.

References

[1] S. Hitz and J. Smith, "Estimating global impacts from climate change." Global Environmental Change, **14** (2004) 201.

[2] K. Abbass et al, "A review of the global climate change impacts, adaptation, and sustainable mitigation measures." Environmental Science Pollution Research, **29** (2022) 42539.

[3] U. Shahzad, "Global Warming: Causes, Effects and Solutions." Durreesamin Journal, **1** (2015) 2204.

[4] Md. Khademul Islam Molla et al, "Analysis of Temperature Change under Global Warming Impact using Empirical Mode Decomposition." International Journal of Information Technology, **3** (2006) 1.

[5] R. K. Pachauri et al., Climate change 2014 synthesis report. contribution of working groups I, II, and III to the fifth assessment report of the Intergovernmental Panel on Climate Change, IPCC, Geneva, Switzerland, 2014.

[6] A. K. Verma and S. Prakash, "Impact of COVID-19 on Environment and Society." Journal of Global Biosciences, **9** (2020) 7352.

[dataset] [7] GISTEMP Team, GISS Surface Temperature Analysis (GISTEMP), version 4. NASA Goddard Institute for Space Studies, 2024. https://data.giss.nasa.gov/gistemp/. - N. Lenssen et al, "Improvements in the GISTEMP uncertainty model. J. Geophysical Research Atmospheres, **124** (2019) 6307. https://doi.org/10.1029/2018JD029522.

[8] NASA GISS, Research features, Why So Many Global Temperature Records? https, ://www.giss.nasa.gov/research/features/201501 _gistemp/, 2015 (accessed 21 January 2015)

[9] Data GISS, GISTEMP, Frequently Asked Questions. https://data.giss.nasa.gov/gistemp/faq, 2016 (accessed 18 August 2016).

[10] C. Maji et al, "Impact of climate change on seismicity: a statistical approach." Arabian Journal Geosciences, **14** (2021) 2725.

[11] M. P. de Souza Echer et al, "On the relationship between global, hemispheric and latitudinal averaged air surface temperature (GISS time series) and solar activity." Journal of Atmospheric and Solar-Terrestrial Physics, **74** (2012) 87.

[12] M. Hasan et al, "ARMA Model Development and Analysis for Global Temperature Uncertainty." Frontiers in Astronomy and Space Sciences, **10** (2023) 1098345.

[13] E. Myrvoll-Nilsen et al, "Warming Trends, and Long-Range Dependent Climate Variability Since The year 1900: A Bayesian Approach." Frontiers in Earth Science, **7** (2019) 214.

[14] F. Yasmeen, "Measuring Global Warming: Global and Hemisphere Mean Temperature Anomalies Predictions Using Sliced Functional Time Series (SFTS) Model." Open Journal of Applied Sciences, **9** (2019) 316.

[15] A. A. Tashilova et al., "Analysis of Climate Change in the Caucasus Region: End of the 20th–Beginning of the 21st Century." Climate, **7** (2019) 11.

[16] U. Triacca and A. Pasini, "Arctic amplification: evidence from a cluster analysis of temperature time series for eight latitude bands." Theoretical and Applied Climatology, **137** (2019) 505.

[17] P. Baranowski et al., "Multifractal analysis of meteorological time series to assess climate impacts." Theoretical and Applied Climatology, **137** (2015) 1811.

[18] R. E. Benestad, "Record-value, non-stationarity tests, and extreme value distributions." Global and Planetary Change, **44** (2004) 11.

[19] K. Rypdal et al., "Long-range memory in Earth's surface temperature on time scales from months to centuries." Journal of Geophysical Research: Atmospheres, **118** (2013) 7046.

[20] A. Phinyomark et al., "Fractal Analysis of Human Gait Variability via Stride Interval Time Series." Frontiers in Physiology **11** (2020) 333.

[21] B. B. Mandelbrot, "How Long Is the Coast of Britain? Statistical Self-Similarity and Fractional Dimension." Science, **165** (1967) 636.

[22] I. Pilgrim, R. P. Taylor, Fractal Analysis of Time-Series Data Sets: Methods and Challenges. In Fractal Analysis, S. Ouadfeul (Ed.), IntechOpen, London, UK, 2019, pp. 5–30.

[23] A. Eke, "Pitfalls in fractal time series analysis: fMRI BOLD as an exemplary case." Frontiers in Physiology, **3** (2012) 417.

[24] J. W. Kantelhardt, Fractal and multifractal time series. In Mathematics of Complexity and Dynamical Systems, R. Meyers (Ed.), Springer, New York, 2012, In: Meyers, pp. 463–87.

[25] S. Kimiagar et al., "Fractal analysis of discharge current fluctuations." Journal of Statistical Mechanics: Theory and Experiment, **3** (2009) 03020.

[26] M. S. Movahed et al., "Multifractal detrended fluctuation analysis of sunspot time series." Journal of Statistical Mechanics: Theory and Experiment, **2** (2006) 02003.